

# Scalable Deep Compressive Sensing

Anonymous authors  
Paper under double-blind review

## Abstract

Deep learning has been used to image compressive sensing (CS) for enhanced reconstruction performance. However, most existing deep learning methods train different models for different subsampling ratios, which brings an additional hardware burden. In this paper, we develop a general framework named scalable deep compressive sensing (SDCS) for the scalable sampling and reconstruction (SSR) of all existing end-to-end-trained models. In the proposed way, images are measured and initialized linearly. Two sampling matrix masks are introduced to flexibly control the subsampling ratios used in sampling and reconstruction, respectively. To achieve a reconstruction model with flexible subsampling ratios, a training strategy dubbed scalable training is developed. In scalable training, the model is trained with the sampling matrix and the initialization matrix at various subsampling ratios by integrating different sampling matrix masks. Experimental results show that models with SDGS can achieve SSR without changing their structure while maintaining good performance, and SDGS outperforms other SSR methods.

## 1 Introduction

Compressive sensing (CS) is a technique that simultaneously samples and compresses signals. And the signal is sampled and reconstructed at a ratio that can be much lower than the Nyquist rate. The sampling process of CS can be expressed as  $\mathbf{y} = \mathbf{Ax}$ , where  $\mathbf{x} \in \mathbb{R}^N$  is the original signal,  $\mathbf{y} \in \mathbb{R}^M$  denotes the measurement,  $\mathbf{A} \in \mathbb{R}^{M \times N}$  is the sampling matrix with  $M < N$  and  $M/N$  is the CS ratio. The signal recovery from  $\mathbf{y}$  is under-determined, and it is usually carried out by solving an optimization problem as follows:

$$\min_{\mathbf{x}} \Re(\mathbf{x}), \text{ s. t. } \mathbf{y} = \mathbf{Ax}, \quad (1)$$

where  $\Re(\mathbf{x})$  is the regularization term. In this paper, we mainly focus on the visual image CS (Lohit et al., 2018a) which has been applied in single-pixel imaging (SPI) (Lohit et al., 2018a; Duarte et al., 2008) and wireless broadcast (Yin et al., 2016; Li et al., 2013; Guo et al., 2020). And since block-by-block sampling and reconstruction (Dong et al., 2014; Dinh & Jeon, 2017; Lohit et al., 2018a; Zhang & Ghanem, 2018; Zhang et al., 2021) would bring less burden to the hardware, we mainly focus on the block-based visual image CS problem.

To solve the problem (1), model-based methods (Dong et al., 2014; Li et al., 2020) introduce various hand-crafted regularizers (Elad, 2010; Liu et al., 2019) and apply non-linear iterative algorithms (Beck & Teboulle, 2009; Donoho et al., 2009) to recover images. These methods usually have theoretical guarantees and work well using sampling matrices with different CS ratios. However, their performance needs to be further improved.

In recent years, deep learning has achieved great success in computer vision (Rick Chang et al., 2017; Dong et al., 2018; Yan et al., 2020a;c;b; Tu et al., 2022; Hu et al., 2021). Among them, models for visual image CS can be cast into two categories: traditional deep learning models and deep unfolding models. Traditional deep learning models (Mousavi et al., 2015; Lohit et al., 2018a; Shi et al., 2019a; 2020) are usually stacked by non-linear computational layers. These models map the measurement to the output without considering the prior information of images. Although they can reconstruct high-quality images at a high speed, there is no good interpretability and theoretical guarantee (Huang et al., 2018). Deep unfolding models denote a

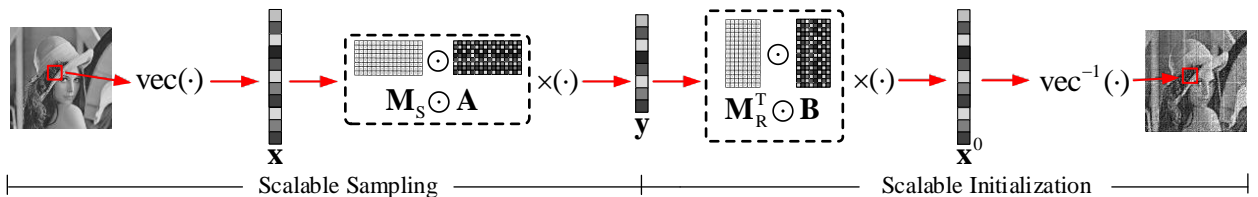


Figure 1: Scalable sampling and scalable initialization of an image block.

series of models constructed by mapping iterative algorithms with unfixed numbers of steps onto deep neural networks with fixed numbers of steps (Gregor & LeCun, 2010; Zhang & Ghanem, 2018; Metzler et al., 2017; Zhang et al., 2021; Dong et al., 2018; Sun et al., 2016; Ma et al., 2019). By combining the interpretability of model-based methods and the trainable characteristics of traditional deep learning models, they make a good balance between reconstruction performance and interpretability.

Usually, the above two kinds of deep-learning-based models are trained end-to-end using some well-known backpropagation algorithms (Kingma & Ba, 2015). However, a common shortage of most existing end-to-end-trained models is that different models have to be trained for different CS ratios. In some applications, sampling and reconstructing images at different CS ratios may be required(Yin et al., 2016; Li et al., 2013). However, storing more than one model with the same structure would bring additional burdens to the hardware. Thus, sampling and reconstructing images at different CS ratios with only one model is needed.

At present, there exist a few methods (Xu et al., 2020; Su & Lian, 2020; Shi et al., 2019b; Zhang et al., 2020; Lohit et al., 2018b; Li et al., 2020) which reconstruct images at different CS ratios using only one model, and they can be roughly cast into two categories. The first kind (Xu et al., 2020; Su & Lian, 2020) trains a single model to adapt to a set of sampling matrices with different CS ratios. The second kind (Shi et al., 2019b; Lohit et al., 2018b) applies only one sampling matrix and integrates its rows to achieve sampling and reconstruction at different CS ratios, and we call such a strategy as **scalable sampling and reconstruction** (SSR) in this paper. This paper focuses on SSR methods, because they are more practical in existing applications such as SPI (Lohit et al., 2018a), wireless broadcasting (Yin et al., 2016), and MRI (Sun et al., 2016). In detail, in image CS for wireless broadcast (Yin et al., 2016; Li et al., 2013), images are reconstructed with different quality according to different channel conditions using one sampling matrix at the receiving end. And in SPI (Lohit et al., 2018a), different CS ratios can be applied for different image quality and sampling time by combining rows of the sampling matrix. However, existing SSR methods cannot be applied universally (Shi et al., 2019b) or a more appropriate sampling matrix is needed (Zhang et al., 2020; Lohit et al., 2018b). Therefore, a general and more effective SSR method is expected.

In this paper, we propose a general framework dubbed **scalable deep compressive sensing** (SDCS) to achieve sampling and reconstructing images at all CS ratios in a certain range. In detail, two binary sampling matrix masks are developed to activate rows of the sampling matrix and the initialization matrix to control the CS ratios for SSR. And we develop a novel training strategy named scalable training, which integrates the multi-ratio information into the training stage by randomly generating sampling matrix masks for different CS ratios. We emphasize that SDCS can bring to the model the ability of SSR, while maintaining the characteristics of its own structure. Furthermore, experimental results show that the model with SDCS can obtain a more effective combination of sampling matrix and model than existing SSR methods.

Our paper has three contributions:

- We propose a framework named SDCS that jointly trains the sampling matrix and the model to achieve sampling and reconstruction at all CS ratios in a certain range.
- With SDCS, a deep learning model can achieve SSR without changing its original structure, while maintaining good performance.
- Technically, SDCS can be used for all end-to-end-trained deep learning models.

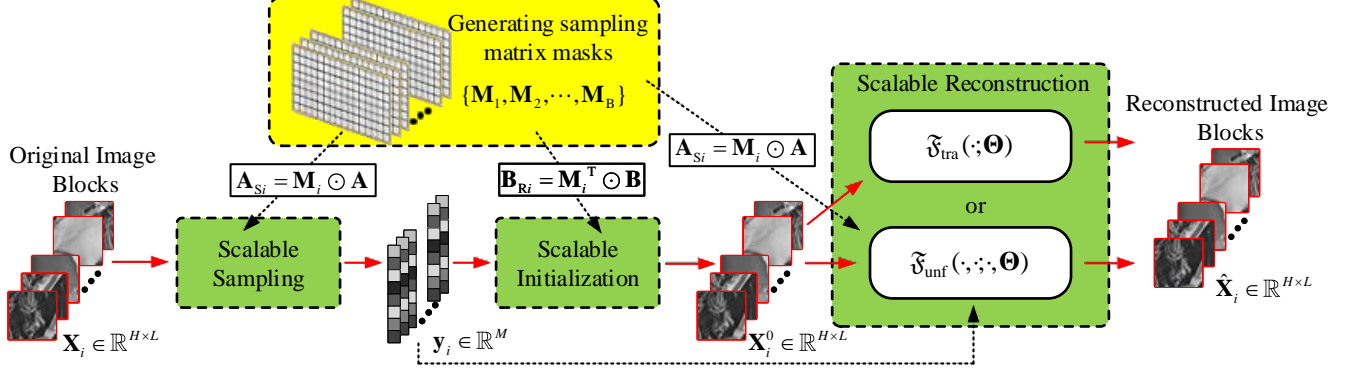


Figure 2: Forward-propagation of the scalable training.

## 2 SDCS

In this section, we introduce the proposed framework SDCS which is simple but powerful. SDCS is composed of four parts: scalable sampling, scalable initialization, scalable reconstruction, and scalable training.

### 2.1 Scalable Sampling

Assume that the largest CS ratio is  $R_M$ , then the sampling matrix can be expressed as  $\mathbf{A} \in \mathbb{R}^{[R_M N] \times N}$ . It can be noticed that the CS ratio is determined by the row number of  $\mathbf{A}$ . Therefore, to achieve scalable sampling, we design a sampling matrix mask  $\mathbf{M}_S \in \mathbb{R}^{[R_M N] \times N}$  to control the activities of the rows of  $\mathbf{A}$ .  $\mathbf{M}_S$  is a zero-one matrix which satisfies  $\mathbf{M}_S(1 : [R_S N], :) = 1$  and  $\mathbf{M}_S([R_S N] + 1 : [R_M N], :) = 0$ , where  $R_S$  denotes the CS ratio for sampling. In such a case, we can generate a new sampling matrix as  $\mathbf{A}_S = \mathbf{M}_S \odot \mathbf{A}$ , where  $\odot$  denotes the element-wise product. Since the  $[R_S N] + 1$ -th row to the  $[R_M N]$ -th row of  $\mathbf{A}_S$  are all filled with 0, we say that the first row to the  $[R_S N]$ -th row of  $\mathbf{A}$  are activated. In detail, if the original image block is  $\bar{\mathbf{X}} \in \mathbb{R}^{H \times L}$  satisfying  $N = HL$ , then the scalable sampling at the CS ratio of  $R_S$  can be expressed as:

$$\mathbf{y} = \mathbf{A}_S \text{vec}(\bar{\mathbf{X}}), \quad (2)$$

where  $\text{vec}(\cdot)$  is an operator which transforms a matrix to a vector and  $\mathbf{y} \in \mathbb{R}^{[R_M N]}$  is the measurement. It can be noticed that  $\mathbf{y}([R_S N] + 1 : [R_M N]) = 0$  and  $\mathbf{y}(1 : [R_S N])$  is the valid measurement for reconstruction. In this way, we can achieve a unified learning mode with different compression rates.

### 2.2 Scalable Initialization

For deep learning methods, the initialized image is important in the following reconstruction. In SDCS, we use a linear operation to initialize the image block.

An initialization matrix  $\mathbf{B} \in \mathbb{R}^{N \times [R_M N]}$  is developed. Similar to (2), a sampling matrix mask  $\mathbf{M}_R \in \mathbb{R}^{[R_M N] \times N}$  is proposed to control the activities of the columns of  $\mathbf{B}$ , where  $\mathbf{M}_R(1 : [R_R N], :) = 1$  and  $\mathbf{M}_R([R_R N] + 1 : [R_M N], :) = 0$ .  $R_R$  denotes the CS ratio for initialization and reconstruction, which satisfies  $R_R \leq R_S$ . In such a case, we can activate the first column to the  $[R_R N]$ -th column of  $\mathbf{B}$  to generate a new initialization matrix as  $\mathbf{B}_R = \mathbf{M}_R^T \odot \mathbf{B}$ . The detailed scalable initialization at the CS ratio of  $R_R$  can be expressed as:

$$\mathbf{X}^0 = \text{vec}^{-1}(\mathbf{B}_R \mathbf{y}), \quad (3)$$

where  $\mathbf{X}^0 \in \mathbb{R}^{H \times L}$  denotes the initialized image block and  $\text{vec}^{-1}(\cdot)$  is the operator which transforms a vector to matrix.

In some cases,  $R_R$  can be lower than  $R_S$ . For example, in wireless broadcasting (Yin et al., 2016), images are transferred at a high CS ratio and are received at a low CS ratio due to the poor channel condition. Fig. 1 illustrates the scalable sampling and scalable initialization of an image.

### 2.3 Scalable Reconstruction

In this subsection, we describe the scalable reconstruction of two different kinds of deep learning models: traditional deep learning models and deep unfolding models.

The generalized reconstruction process of traditional deep learning models can be expressed as:

$$\hat{\mathbf{X}} = \mathfrak{F}_{\text{tra}}(\mathbf{X}^0; \Theta), \quad (4)$$

where  $\hat{\mathbf{X}} \in \mathbb{R}^{H \times L}$  is the reconstructed image block and  $\Theta$  contains trainable parameters of the model. In SDCS,  $\Theta$  is trained with  $\mathbf{A}$  and  $\mathbf{B}$  to make sure that  $\mathfrak{F}_{\text{tra}}(\cdot; \Theta)$  can perform well at all CS ratios.

The reconstruction model of a deep unfolding model is usually composed of  $K$  reconstruction modules with the same structure. In each module, the sampling matrix also participates in the image reconstruction. In detail, the generalized reconstruction process of a deep unfolding model can be expressed as:

$$\hat{\mathbf{X}} = \mathfrak{F}_{\text{unf}}(\mathbf{X}^0, \mathbf{y}; \mathbf{A}, \Theta) = \mathfrak{F}_{\text{unf}}^K(\mathbf{X}^{K-1}, \mathbf{y}; \mathbf{A}, \Theta^K), \quad (5)$$

$$\mathbf{X}^k = \mathfrak{F}_{\text{unf}}^k(\mathbf{X}^{k-1}, \mathbf{y}; \mathbf{A}, \Theta^k), \quad (6)$$

where  $\mathfrak{F}_{\text{unf}}(\cdot, \cdot; \mathbf{A}, \Theta)$  is the entire deep unfolding model, of which  $\Theta$  contains its trainable parameters.  $\mathfrak{F}_{\text{unf}}^k(\cdot, \cdot; \mathbf{A}, \Theta^k)$  is the  $k$ -th reconstruction module and  $\Theta^k$  contains its trainable parameters. the inputs of  $\mathfrak{F}_{\text{unf}}(\cdot, \cdot; \mathbf{A}, \Theta)$  and  $\mathfrak{F}_{\text{unf}}^k(\cdot, \cdot; \mathbf{A}, \Theta^k)$  usually contain the image block  $\mathbf{X}^0$  and the measurement  $\mathbf{y}$ . Since  $\mathbf{A}$  plays an important role in each reconstruction module, the scalable reconstruction of the deep unfolding model is achieved by applying an activated sampling matrix. In detail, the scalable reconstruction of the  $k$ -th reconstruction model can be expressed as:

$$\mathbf{X}^k = \mathfrak{F}_{\text{unf}}^k(\mathbf{X}^{k-1}, \mathbf{y}; \mathbf{M}_R \odot \mathbf{A}, \Theta^k). \quad (7)$$

Similar to the traditional deep learning models,  $\Theta = \{\Theta^1, \Theta^2, \dots, \Theta^K\}$  is trained with  $\mathbf{A}$  and  $\mathbf{B}$ . Since the sampling matrix  $\mathbf{A}$  usually appears in the image sampling and reconstruction of deep unfolding models, deep unfolding models have great potential to achieve SSR.

### 2.4 Scalable Training

As shown in (2), (3) and (7),  $\mathbf{A}$  and  $\mathbf{B}$  are important in effective SSR. How to obtain an appropriate combination of  $\mathbf{A}$ ,  $\mathbf{B}$  and the reconstruction model is the main issue. To this end, we develop a novel training strategy dubbed scalable training to train  $\mathbf{A}$ ,  $\mathbf{B}$  with parameters of the reconstruction model jointly.

In scalable training, it is assumed that all parameters are trained using stochastic-gradient-descent-related algorithms like Adam (Kingma & Ba, 2015). If the batch size for training is  $B$  and the loss function is  $L$ , the training process of  $\mathbf{A}$ ,  $\mathbf{B}$  and  $\Theta$  of one epoch can be expressed as Algorithm 1. And Fig. 2 illustrates the forward-propagation of the scalable training. The gradients of  $\mathbf{A}$  and  $\mathbf{B}$  can be computed as follows:

$$\nabla_{\mathbf{A}} L = \frac{1}{B} \sum_{i=1}^B \mathbf{M}_i \odot \nabla_{\mathbf{M}_i \odot \mathbf{A}} L, \quad (8)$$

$$\nabla_{\mathbf{B}} L = \frac{1}{B} \sum_{i=1}^B \mathbf{M}_i^T \odot \nabla_{\mathbf{M}_i^T \odot \mathbf{B}} L. \quad (9)$$

It can be noticed that the closer to the top of  $\mathbf{A}$  or the left of  $\mathbf{B}$ , the more gradient information for updating is obtained, which makes using  $\mathbf{M}_S$  and  $\mathbf{M}_R$  for effective SSR possible. It is emphasized that the form of  $L$  is not limited by SDCS, but related to the combined reconstruction model.

---

**Algorithm 1** Scalable training of one epoch.

**Input:** training set  $\mathbb{T}$ , batch size  $B$ , loss function  $L$ , max CS ratio  $R_M$ , sampling matrix  $\mathbf{A}$ , initialization matrix  $\mathbf{B}$ , reconstruction model  $\mathfrak{F}_{\text{tra}}(\cdot; \Theta)$  or  $\mathfrak{F}_{\text{unf}}(\cdot; \mathbf{A}, \Theta)$ .

**Output:** trained parameters.

```

1:  $\mathbb{T}' \leftarrow \emptyset$ 
2: repeat
3:   Select  $\mathbb{S} = \{\mathbf{X}_1, \mathbf{X}_2, \dots, \mathbf{X}_B\} \in \mathbb{T} \setminus \mathbb{T}'$ .
4:    $\mathbb{T}' \leftarrow \mathbb{T}' \cup \mathbb{S}$ .
5:   Generate  $\{R_1, R_2, \dots, R_B\}$  randomly, where  $R_i \in [1, R_M]$ .
6:   Generate  $\{\mathbf{M}_1, \mathbf{M}_2, \dots, \mathbf{M}_B\}$ , where  $\mathbf{M}_i(1 : \lceil R_i N \rceil, :) = 1$  and  $\mathbf{M}_i(\lceil R_i N \rceil + 1 : \lceil R_M N \rceil, :) = 0$ .
7:   Generate  $\mathbb{A}_S = \{\mathbf{A}_{S1}, \mathbf{A}_{S2}, \dots, \mathbf{A}_{SB}\}$ ,  $\mathbb{A}_R = \{\mathbf{A}_{R1}, \mathbf{A}_{R2}, \dots, \mathbf{A}_{RB}\}$  and  $\mathbb{B}_R = \{\mathbf{B}_{R1}, \mathbf{B}_{R2}, \dots, \mathbf{B}_{RB}\}$ ,  
where  $\mathbf{A}_{Si} = \mathbf{M}_i \odot \mathbf{A}$ ,  $\mathbf{A}_{Ri} = \mathbf{M}_i \odot \mathbf{A}$  and  $\mathbf{B}_{Ri} = \mathbf{M}_i^T \odot \mathbf{B}$ .
8:   for  $i = 1 : B$  do
9:      $\mathbf{y}_i = \mathbf{A}_{Si} \text{vec}(\mathbf{X}_i)$ 
10:     $\mathbf{X}_i^0 = \text{vec}^{-1}(\mathbf{B}_{Ri} \mathbf{y}_i)$ 
11:     $\hat{\mathbf{X}}_i = \mathfrak{F}_{\text{tra}}(\mathbf{X}_i^0; \Theta)$  or  $\hat{\mathbf{X}}_i = \mathfrak{F}_{\text{unf}}(\mathbf{X}_i^0, \mathbf{y}_i; \mathbf{A}_{Ri}, \Theta)$ 
12:    Compute loss  $L$  using  $\{\hat{\mathbf{X}}_1, \hat{\mathbf{X}}_2, \dots, \hat{\mathbf{X}}_B\}$  and  $\mathbb{S}$ .
13:    Update  $\mathbf{A}$ ,  $\mathbf{B}$  and  $\Theta$ .
14: until  $\mathbb{T} \setminus \mathbb{T}' = \emptyset$ 
15: return  $\mathbf{A}$ ,  $\mathbf{B}$ ,  $\Theta$ .

```

---

Furthermore, to validate the trained model, a CS ratio validation group (RVG) is applied. Each RVG contains  $G$  validation CS ratios as  $\{R_1, R_2, \dots, R_G\}$ . At the end of each epoch, for each ratio  $R_i$ , the average PSNR on the validation set can be obtained. And the model with the best average PSNR on RVG is regarded as the model for test.

We emphasize that SDCS has no restriction on the structure of deep learning models, which means it can be combined with any end-to-end-trained model for SSR. However, the final performance is determined by the structure of the reconstruction model.

### 3 Related Works

In this section, we first introduce some deep-learning-based methods for image CS, then some SSR methods are compared with SDCS.

#### 3.1 Deep Learning Models for Image CS

For traditional deep learning models, Mousavi et al. (Mousavi et al., 2015) first designed a fully-connected-layer-based stacked denoising autoencoder (SDA) for visual image CS. Lohit et al. (Lohit et al., 2018a) first proposed a six-layers CNN-based model named ReconNet to reconstruct image blocks from measurements. Shi et al. (Shi et al., 2019a) proposed a deeper CNN model named CSNet which has trainable deblocking operations and integrated residual connection (He et al., 2016) for better performance. Furthermore, there are some other models (Du et al., 2019; Yao et al., 2019; Bora et al., 2017; Sun et al., 2020) for visual image CS, and all these models have one thing in common the models for reconstruction are trained end-to-end.

Deep unfolding models are first developed for the sparse coding problem (Gregor & LeCun, 2010; Chen et al., 2018; Borgerding et al., 2017). And inspired by these models, Zhang et al. (Zhang & Ghanem, 2018) developed a deep unfolding model named ISTA-Net for image CS problem by unfolding iterative shrinkage-thresholding algorithm (ISTA) and learning sparse transformation functions. Metzler et al. (Metzler et al., 2017) and Zhang et al. (Zhang et al., 2021) established deep unfolding models named LDAMP and AMP-Net respectively based on approximate message passing (AMP) algorithm, where LDAMP samples and reconstructs the entire image, and AMP-Net measures and recovers an image block-by-block with general trainable deblocking modules. Dong et al. (Dong et al., 2018) designed a model named DPDNN inspired

by the half-quadratic splitting (HQS) algorithm for image inverse problems which can be applied to visual image CS. These deep unfolding models apply the sampling matrix for reconstruction and they can also be trained end-to-end.

Some of the above methods discuss the sampling matrix training strategies, including in traditional deep learning models (Mousavi et al., 2015; Shi et al., 2019a) or in the deep unfolding model (Zhang et al., 2021), and they all train their initialization matrices. Although the trained sampling matrices can improve the reconstruction performance, they are designed for the single CS ratio and the performance would decrease seriously when the CS ratio changes for SSR. However, using SDCS, the model and the trained sampling matrix can perform well in all CS ratios in a certain range.

### 3.2 SSR Methods

As far as we know, there exist several SSR methods (Shi et al., 2019b; Lohit et al., 2018b; Zhang et al., 2020). We introduce and compare them with SDCS in the following paragraphs.

Shi et al. (Shi et al., 2019b) proposed a model dubbed SCSNet. SCSNet trains the sampling matrix with the reconstruction model which is composed of seven independent sub-models with the same structure. Each sub-model adapts with a sub-range of CS ratios to make sure that the whole model can achieve SSR at CS ratios from 1% to 50%. And a greedy algorithm is applied to rearrange the rows of the sampling matrix for better reconstruction. However, SCSNet has two weaknesses: 1) The number of parameters is very large due to the existence of multiple sub-models. 2) Based on SCSNet, the existing deep learning models have to change their structure to achieve scalable reconstruction which would bring more burden to the hardware. However, SDCS needs only one model to achieve SSR and it can be applied to all end-to-end-trained models without changing their structures.

Zhang et al. (Zhang et al., 2020) propose a framework named CRA which applies two reconstruction models, of which the first one is for initializing and completing the measurement, and the second one is for further reconstruction. Compared with SDCS, CRA do not train the sampling matrix, and two reconstruction models would introduce more parameters. Furthermore, we emphasize that CRA is essentially a pluggable method, which can be combined with other SSR methods by applying a non-linear model for initialization and measurement completion. Therefore, the experimental comparison between SDCS and CRA is not the focus of our paper.

Lohit et al. (Lohit et al., 2018b) designed a general framework like SDCS named Rate-Adaptive CS (RACS) which does not need to change the structure of the model, and it has three training stages. In stage 1, the model is trained with the sampling matrix at a single CS ratio of  $R_M$ . And all parameters of the model are frozen after stage 1. In stage 2, The first  $R_K N$  rows of the sampling matrix are optimized, where  $R_K < R_M$ . In stage 3, the following rows of the sampling matrix are trained one by one. It can be noticed that RACS has an obvious weakness: the model is learned for a specific sampling matrix with CS ratio  $R_M$  in stage 1, which means the performance of the model at lower CS ratios can be further improved. Different from RACS, with SDCS, the learned model adapts to a sampling matrix that can change its CS ratios from 1% to  $R_M$  using a sampling matrix mask. Our strategy brings the model the potential that performs better for SSR.

## 4 Experimental Results

### 4.1 Experimental settings

In this paper, the model combined with SDCS is named as *model*-SDCS. To evaluate the performance of SDCS, six models are combined with SDCS, namely SDA (Mousavi et al., 2015), ReconNet (Lohit et al., 2018a), CSNet<sup>+</sup> (Shi et al., 2019a), ISTA-Net<sup>+</sup> (Zhang & Ghanem, 2018), DPDNN (Dong et al., 2018) and AMP-Net (Zhang et al., 2021), which sample and reconstruct images block-by-block with the block size of  $33 \times 33$  that makes  $N = 1089$ . SDA, ReconNet, CSNet<sup>+</sup> are traditional deep learning models. ISTA-Net<sup>+</sup>, DPDNN and AMP-Net are deep unfolding models with 9, 6 and 6 reconstruction modules respectively. In this paper, the activation functions of SDA are changed to the Rectified Linear Unit (ReLU) (Lohit et al., 2018a)

for better performance. It is worth noting that in CSNet<sup>+</sup> and AMP-Net, trainable deblocking operations are applied and the sampling matrices are trained for a single CS ratio. Furthermore, since SCSNet (Shi et al., 2019b) and RACS (Lohit et al., 2018b) can achieve SSR like *model*-SDCS, they are compared with SDCS to show the effectiveness of our framework.

All of our experiments are performed on two datasets: BSDS500 (Arbelaez et al., 2010) and Set11 (Lohit et al., 2018a). BSDS500 contains 500 colorful visual images and is composed of a training set (200 images), a validation set (100 images) and a test set (200 images). Set11 (Lohit et al., 2018a) contains 11 grey-scale images. In this paper, BSDS500 is used for training, validation and testing. And Set11 is used for testing. We generate two training sets for models with and without trainable deblocking operations. (a) Training set 1 contains 89600 sub-images sized of  $99 \times 99$  which are randomly extracted from the luminance components of images in the training set of BSDS500 (Shi et al., 2019a). (b) Training set 2 contains 195200 sub-images sized of  $33 \times 33$  which are randomly extracted from the luminance components of images in the training set of BSDS500 (Zhang & Ghanem, 2018). In this paper, CSNet<sup>+</sup>, AMP-Net, CSNet<sup>+</sup>-SDCS, AMP-Net-SDCS and SCSNet are trained on training set 1 due to the existence of trainable deblocking operations. SDA, ReconNet, ISTA-Net<sup>+</sup>, DPDNN, SDA-SDCS, ReconNet-SDCS, ISTA-Net<sup>+</sup>-SDCS and DPDNN-SDCS are trained on training set 2. And they are trained on the conditions in their original papers. Moreover, we use the validation set of BSDS500 for model choosing and the test set of BSDS500 for testing. In this paper, all sampling matrices are initialized randomly in Gaussian distribution.  $R_M$  is 50% and RVG is {1%, 4%, 10%, 25%, 30%, 40%, 50%}. All experiments are performed on a computer with an AMD Ryzen7 2700X CPU and an RTX2080Ti GPU.

## 4.2 Comparison with original deep learning methods

In this subsection, we compare SDA, ReconNet, CSNet<sup>+</sup>, ISTA-Net<sup>+</sup>, DPDNN and AMP-Net with SDA-SDCS, ReconNet-SDCS, CSNet<sup>+</sup>-SDCS, ISTA-Net<sup>+</sup>-SDCS, DPDNN-SDCS and AMP-Net-SDCS. AMP-Net-SDCS\* represents the experimental results that sampling matrix **A** and initialization matrix **B** are not involved in training. Table 1 and Table 2 show the average PSNR and SSIM of 12 models tested on Set11 and the testing set of BSDS500 at different CS ratios respectively. We emphasize that there are seven different models for seven different test CS ratios for the method without SDCS, and a single model is tested at different CS ratios for *model*-SDCS.

Table 1: The results of twelve models tested on Set11 at different CS ratios, where the best is marked in bold.

Method	50%	40%	30%	25%	10%	4%	1%
	PSNR (dB)/SSIM						
SDA	26.43/0.8007	25.14/0.7371	24.77/0.7191	24.77/0.7234	23.66/0.6794	21.05/0.5720	17.69/0.4376
SDA-SDCS	<b>30.80/0.9038</b>	<b>30.63/0.9009</b>	<b>29.43/0.8793</b>	<b>28.76/0.8636</b>	<b>25.58/0.7660</b>	<b>22.77/0.6458</b>	<b>19.87/0.4829</b>
ReconNet	32.12/0.9137	30.59/0.8928	28.72/0.8517	28.04/0.8303	24.07/0.6958	21.00/0.5817	17.54/0.4426
ReconNet-SDCS	<b>34.29/0.9532</b>	<b>33.81/0.9242</b>	<b>32.42/0.9313</b>	<b>31.42/0.9173</b>	<b>26.90/0.8225</b>	<b>23.57/0.6931</b>	<b>20.02/0.5071</b>
CSNet <sup>+</sup>	<b>38.19/0.9739</b>	<b>36.15/0.9625</b>	<b>33.90/0.9449</b>	<b>32.76/0.9322</b>	27.76/0.8513	<b>24.24/0.7412</b>	20.09/0.5334
CSNet <sup>+</sup> -SDCS	36.65/0.9645	35.48/0.9568	33.58/0.9414	32.44/0.9295	<b>27.85/0.8493</b>	23.92/0.7303	<b>20.32/0.5394</b>
ISTA-Net <sup>+</sup>	<b>38.08/0.9680</b>	<b>35.93/0.9537</b>	<b>33.66/0.9330</b>	<b>32.27/0.9167</b>	25.93/0.7840	21.14/0.5947	17.48/0.4403
ISTA-Net <sup>+</sup> -SDCS	36.51/0.9693	34.92/0.9587	32.85/0.9400	31.65/0.9256	<b>26.99/0.8334</b>	<b>23.57/0.7073</b>	<b>20.13/0.5146</b>
DPDNN	35.85/0.9532	34.30/0.9411	32.06/0.9145	30.63/0.8924	24.53/0.7392	21.11/0.6029	17.59/0.4459
DPDNN-SDCS	<b>39.50/0.9775</b>	<b>37.61/0.9686</b>	<b>35.38/0.9543</b>	<b>34.12/0.9434</b>	<b>29.07/0.8708</b>	<b>25.08/0.7622</b>	<b>20.55/0.5423</b>
AMP-Net	<b>40.27/0.9804</b>	<b>38.23/0.9713</b>	<b>35.90/0.9574</b>	34.59/0.9477	29.45/0.8787	25.16/0.7692	<b>20.57/0.5639</b>
AMP-Net-SDCS*	34.57/0.9427	32.89/0.9249	30.12/0.8922	29.32/0.8688	24.99/0.7201	21.21/0.5649	18.97/0.4561
AMP-Net-SDCS	39.67/0.9781	37.96/0.9703	35.89/0.9576	<b>34.67/0.9477</b>	<b>29.59/0.8792</b>	<b>25.43/0.7750</b>	20.47/0.5629

From Table 1 and Table 2, it can be found that compared with models without trained sampling matrices, although *model*-SDCS has only one model for reconstruction, it obtains better performance in terms of PSNR and SSIM at most test CS ratios. And compared with models that also apply trained sampling matrices (CSNet<sup>+</sup> and AMP-Net), *model*-SDCS can still obtain competitive performance at all test CS ratios with only a single model. Such a result implies the great potential of deep learning techniques and the sampling

Table 2: The results of twelve models tested on the test set of BSDS500 at different CS ratios, where the best is marked in bold.

Method	50%	40%	30%	25%	10%	4%	1%
	PSNR (dB)/SSIM						
SDA	26.16/0.8048	24.97/0.7392	24.58/0.7127	24.58/0.7107	23.77/0.6489	21.75/0.5534	19.05/0.4522
SDA-SDCS	<b>30.17/0.9026</b>	<b>29.90/0.8973</b>	<b>28.77/0.8704</b>	<b>28.13/0.8510</b>	<b>25.43/0.7338</b>	<b>23.38/0.6145</b>	<b>21.08/0.4865</b>
ReconNet	30.85/0.8949	29.47/0.8647	27.95/0.8190	27.20/0.7914	23.98/0.6472	21.69/0.5557	18.96/0.4531
ReconNet-SDCS	<b>33.27/0.9448</b>	<b>32.52/0.9355</b>	<b>31.04/0.9107</b>	<b>30.13/0.8921</b>	<b>26.46/0.7753</b>	<b>23.99/0.6502</b>	<b>21.20/0.5063</b>
CSNet <sup>+</sup>	<b>35.89/0.9677</b>	<b>33.96/0.9513</b>	<b>31.94/0.9251</b>	<b>30.91/0.9067</b>	<b>27.01/0.7949</b>	<b>24.41/0.6747</b>	21.42/0.5261
CSNet <sup>+</sup> -SDCS	34.91/0.9588	33.59/0.9462	31.80/0.9221	30.82/0.9043	26.97/0.7906	24.21/0.6692	<b>21.48/0.5288</b>
ISTA-Net <sup>+</sup>	<b>34.92/0.9510</b>	32.87/0.9264	30.77/0.8901	29.64/0.8638	25.11/0.7124	21.82/0.5661	18.92/0.4529
ISTA-Net <sup>+</sup> -SDCS	34.85/0.9622	<b>33.26/0.9465</b>	<b>31.38/0.9199</b>	<b>30.36/0.9003</b>	<b>26.56/0.7811</b>	<b>24.00/0.6555</b>	<b>21.24/0.5096</b>
DPDNN	33.56/0.9373	32.05/0.9164	29.98/0.8759	28.87/0.8491	24.37/0.6863	21.80/0.5716	18.97/0.4544
DPDNN-SDCS	<b>36.84/0.9708</b>	<b>34.91/0.9560</b>	<b>32.85/0.9323</b>	<b>31.74/0.9150</b>	<b>27.58/0.8069</b>	<b>24.78/0.6858</b>	<b>21.72/0.5319</b>
AMP-Net	<b>37.48/0.9744</b>	<b>35.34/0.9594</b>	<b>33.17/0.9358</b>	32.01/0.9188	27.82/0.8133	24.95/0.6949	<b>21.90/0.5501</b>
AMP-Net-SDCS	37.04/0.9720	35.18/0.9580	33.14/0.9354	<b>32.04/0.9187</b>	<b>27.84/0.8136</b>	<b>25.03/0.6967</b>	21.87/0.5493

matrix training strategy. Therefore, we conclude that *model*-SDCS can effectively achieve SSR without changing the structure of the model.

Furthermore, it can be noticed from Table 1 and Table 2 that the above models combined with SDCS can have a good performance of SSR, which verifies the universality of SDCS. It is worth emphasizing that the purpose of the universality of SDCS is not to combine SDCS with all existing models, but to bring reconstruction models the effective SSR performance. This means that researchers can design reconstruction models at a single CS ratio. To achieve SSR, they only need to combine these models with SDCS.

In addition, Table 1 and Table 2 also verify the benefits of the sampling matrix after scalable training, which can be summarized into two points: 1) The trained sampling matrix can improve the performance of the reconstruction model, comparing models with SDCS and without SDCS. 2) The trained sampling matrix can adapt the reconstructed model to different CS ratios.

### 4.3 Comparison with SSR methods

In this subsection, we compare SDCS with two SSR methods: SCSNet (Shi et al., 2019b) and RACS (Lohit et al., 2018b).

Table 3: Parameter number of the reconstruction model of seven models.

Parameter Number	SDA-SDCS	ReconNet-SDCS	CSNet <sup>+</sup> -SDCS	ISTA-Net <sup>+</sup> -SDCS	DPDNN-SDCS	AMP-Net-SDCS	SCSNet
	6534	22914	370560	336978	1363712	229254	1110823

First, SCSNet is compared with SDA-SDCS, ReconNet-SDCS, CSNet<sup>+</sup>-SDCS, ISTA-Net<sup>+</sup>-SDCS, DPDNN-SDCS and AMP-Net-SDCS. Table 3 shows the parameter number of the seven models. Fig. 3 plots the average PSNR and SSIM of the seven models tested on the test set of BSDS500 at CS ratios from 1% to 50%. It can be noticed that except for DPDNN-SDCS, other models have fewer parameters than SCSNet and achieve SSR. And DPDNN-SDCS and AMP-Net-SDCS even outperform SCSNet, which shows the great potential of SDCS. Furthermore, deep unfolding models have better SSR performance than traditional deep learning models. For examples, AMP-Net-SDCS and DPDNN-SDCS outperform SDA-SDCS, ReconNet-SDCS and CSNet<sup>+</sup>-SDCS, and ISTA-Net<sup>+</sup>-SDCS outperform SDA-SDCS and ReconNet-SDCS. we conclude that deep unfolding models are more suitable for SSR to a certain degree due to the important role of the sampling matrix in the image reconstruction process.

Second, SDCS is compared with RACS. Since with SDCS, AMP-Net outperforms other deep unfolding models and CSNet<sup>+</sup> outperforms other traditional deep learning models, we use AMP-Net and CSNet<sup>+</sup> as examples to compare SDCS and RACS. In this subsection, the values of  $R_K$  of RACS mentioned in 3.2 are 1%, 10% and 25%. Fig. 4 plots average PSNR and SSIM of AMP-Net-SDCS, CSNet<sup>+</sup>-SDCS, AMP-Net-RACS- $R_K$

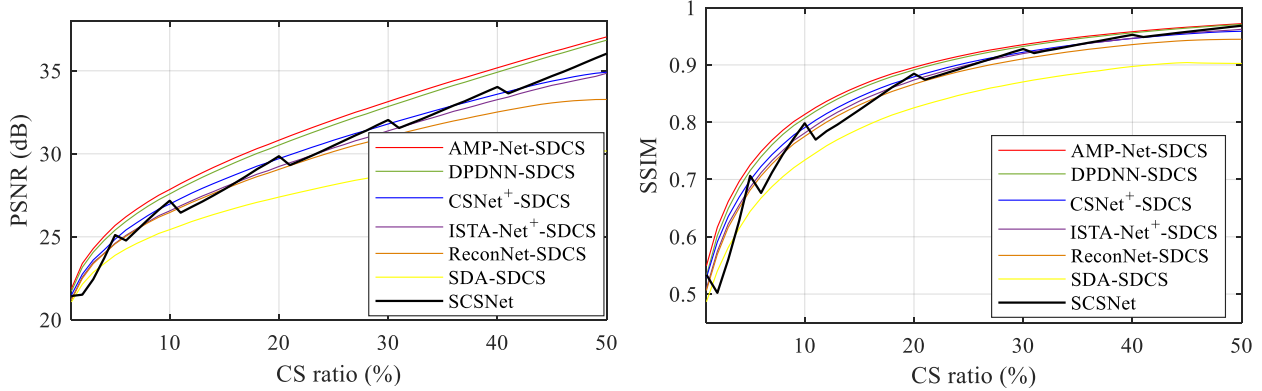


Figure 3: Comparison between SCSNet and six models with SDCS at different CS ratios.

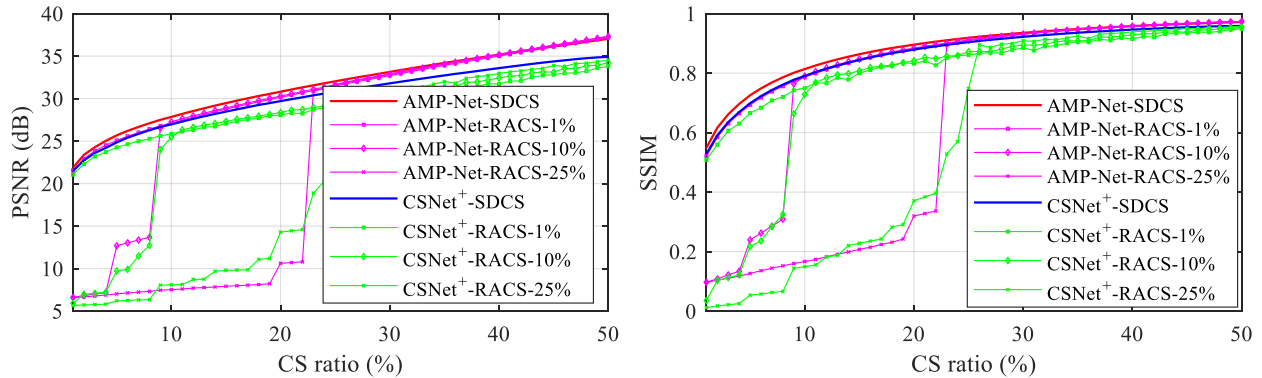
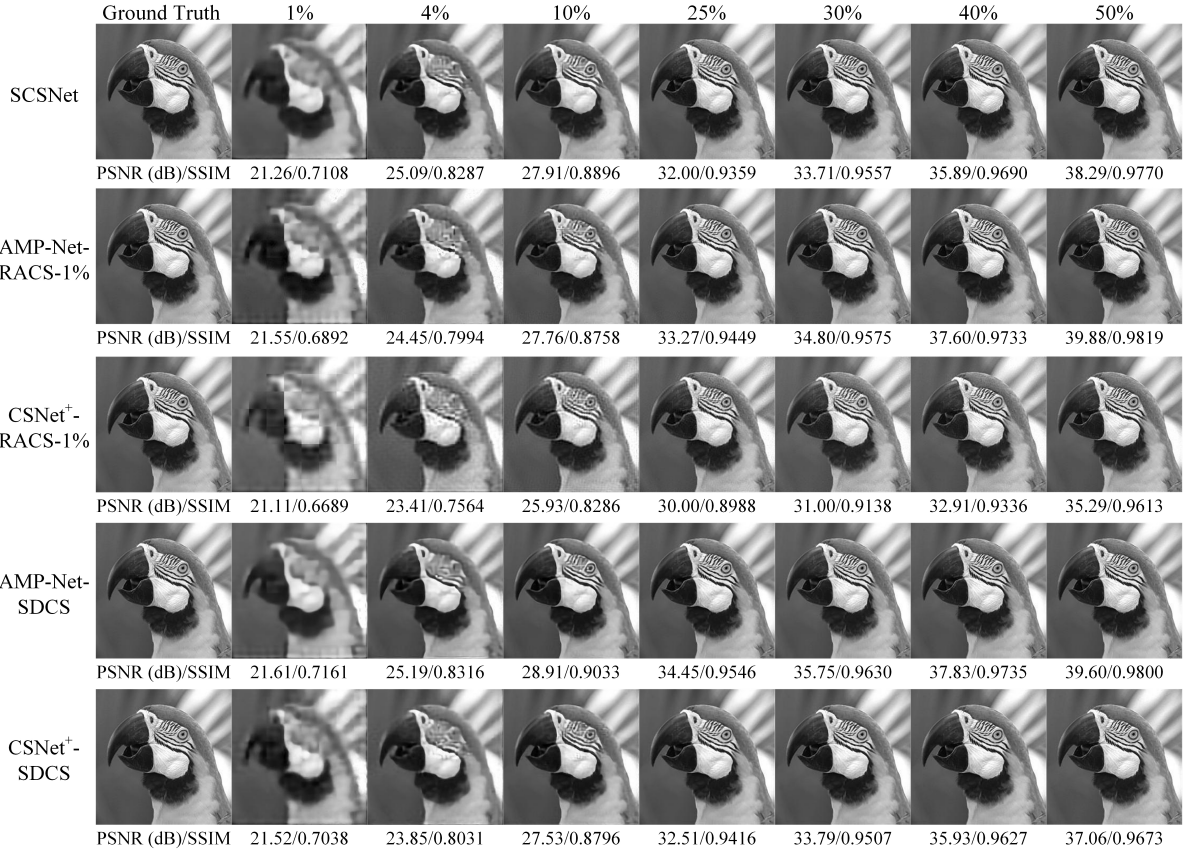


Figure 4: Comparison between SDCS and RACS at different CS ratios.

and  $\text{CSNet}^+ \text{-RACS-}R_K$  on the test set of BSDS500 at CS ratios from 1% to 50%, where  $\text{model-RACS-}R_K$  denotes the model combined with RACS with the hyperparameter  $R_K$ . It can be noticed that when the CS ratio is lower than  $R_K$ ,  $\text{model-RACS-}R_K$  has bad performance. For AMP-Net, AMP-Net-SDCS outperforms all compared AMP-Net-RACS- $R_K$ s when the CS ratio is lower than 30%. And for CSNet+, CSNet+-SDCS has better performance than all compared CSNet+-RACS- $R_K$ s at all CS ratios. Such a result implies that SDCS can generate a more appropriate combination of sampling matrix and model than RACS.

Fig. 5 shows the *Parrots* images in Set11 reconstructed by different SSR models at different CS ratios. Fig. 5 is quite revealing in several ways. 1) AMP-Net-SDCS generates better results than SCSNet while maintaining fewer parameters which shows the great potential of SDCS. 2) *Model-RACS- $R_K$*  can not inherit the characteristics of original models well. For example, AMP-Net and CSNet+ both have trainable deblocking operations, but AMP-Net-RACS-1% and CSNet+-RACS-1% generates images with obvious blocking artifacts at CS ratios of 1%, 4% and 10%. However, AMP-Net-SDCS and CSNet+-SDCS generate smooth images without blocking artifacts. Therefore, we conclude that models with SDCS can get good SSR performance. In particular, they can inherit the characteristics of original models.

To further prove the effectiveness of SDCS, we compare AMP-Net-SDCS and CSNet+-SDCS with AMP-Net and CSNet+ which train their sampling matrices for one single CS ratio and apply the greedy algorithm in SCSNet (Shi et al., 2019b). In this subsection, the sampling matrices of AMP-Net and CSNet+ are trained for the CS ratio of 50%. And their rows are rearranged using the greedy algorithm in SCSNet (Shi et al., 2019b) for better SSR. Fig. 6 plots the average PSNR and SSIM of four models tested on the test set of BSDS500 at CS ratios from 1% to 50%. It can be noticed that at the CS ratio of 50%, the specially trained models can obtain better results than the models with SDCS, but such models have a bad performance at

Figure 5: The *Parrots* images in Set11 Reconstructed by different SSR methods at different CS ratios.

other CS ratios. However, models combined with SDCS perform well at all CS ratios. Therefore, we conclude that *model*-SDCS outperforms the model with a trained sampling matrix for a single CS ratio, and SDCS provides a more obvious improvement than the greedy algorithm of SCSNet under the condition of only one reconstruction model.

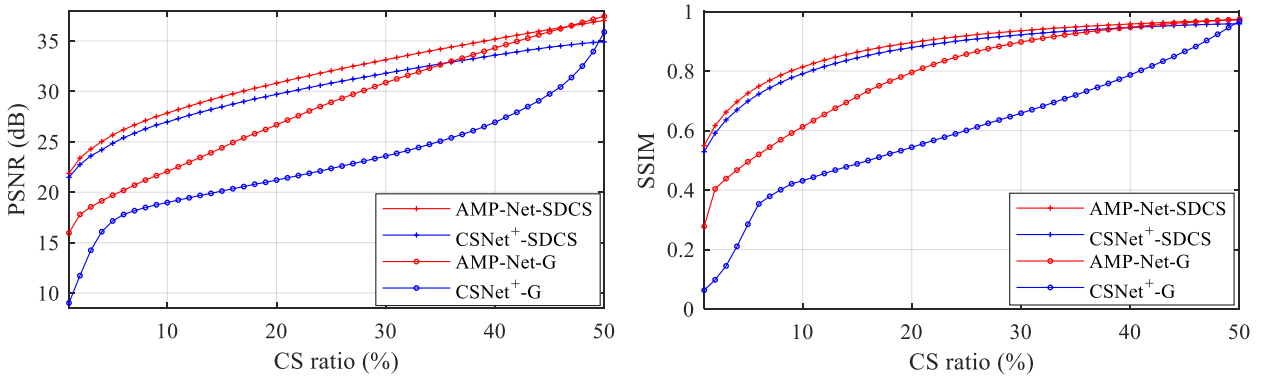
Figure 6: Comparison between two models with and without SDCS at different CS ratios. *model*-G is the model combined with the greedy algorithm in (Shi et al., 2019b).

Table 4: The results of different models on the test set of BSDS500 with different SNRs.

SNR	Method	30%	10%	4%
		PSNR (dB)/SSIM		
40dB	CSNet <sup>+</sup>	31.89/0.9212	27.00/0.7942	24.51/0.6767
	CSNet <sup>+</sup> -SDCS	31.76/0.9219	27.03/0.7953	24.41/0.6768
	AMP-Net	32.93/0.9314	27.73/0.8088	24.94/0.6930
	AMP-Net-SDCS	32.83/0.9301	27.71/0.8083	24.95/0.6916
30dB	CSNet <sup>+</sup>	31.58/0.9145	26.93/0.7863	24.43/0.6714
	CSNet <sup>+</sup> -SDCS	31.62/0.9178	26.95/0.7902	24.30/0.6720
	AMP-Net	31.40/0.9002	26.97/0.7761	24.46/0.6689
	AMP-Net-SDCS	31.61/0.9054	27.12/0.7818	24.57/0.6701
25dB	CSNet <sup>+</sup>	30.87/0.8963	26.46/0.7665	24.12/0.6550
	CSNet <sup>+</sup> -SDCS	30.92/0.9023	26.66/0.7775	24.03/0.6624
	AMP-Net	29.83/0.8588	26.07/0.7328	23.82/0.6350
	AMP-Net-SDCS	29.90/0.8599	26.15/0.7349	23.78/0.6254
15dB	CSNet <sup>+</sup>	26.84/0.7618	23.85/0.6337	21.69/0.5280
	CSNet <sup>+</sup> -SDCS	26.49/0.7492	24.15/0.6434	22.04/0.5479
	AMP-Net	26.43/0.8007	23.21/0.6003	21.66/0.5324
	AMP-Net-SDCS	25.29/0.6936	22.64/0.5486	20.52/0.4433

#### 4.4 Simulating the actual imaging conditions

In some practical conditions, noises may be introduced to the measurement  $\mathbf{y}$ . To this end, we validate the anti-noise performance of SDCS in this subsection to simulate the actual CS imaging conditions. In detail, additive Gaussian white noises (Lepskii, 1991) are added to  $\mathbf{y}$  of all datasets to train and test models in the subsection. And the signal-to-noise ratios (SNRs) are 40dB, 30dB, 25dB and 15dB. All results are obtained by testing 5 times on the test set and averaging.

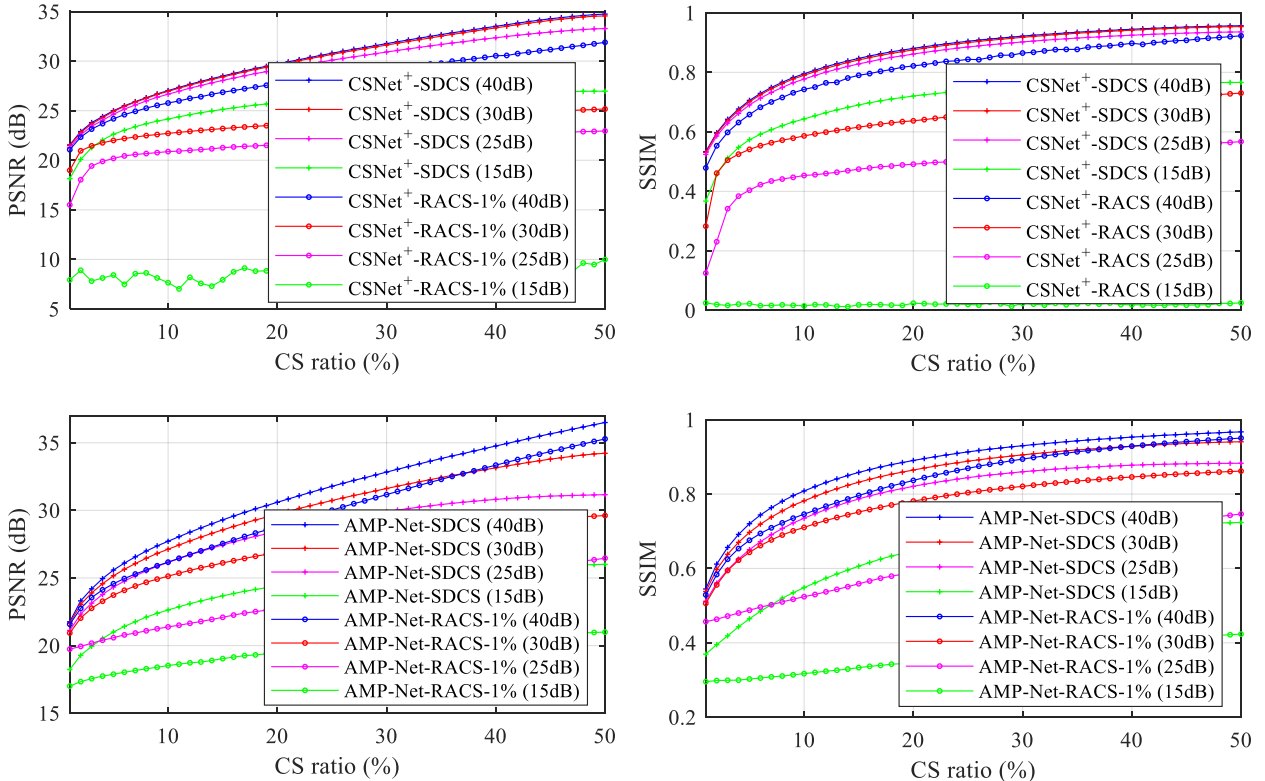


Figure 7: Comparison between SDCS and RACS with different SNRs.

Since with SDCS, AMP-Net outperforms the other deep unfolding models, and CSNet<sup>+</sup> outperforms other traditional deep learning models, we use AMP-Net and CSNet<sup>+</sup> as examples to validate the anti-noise performance of SDCS. Table 4 shows the average PSNR and SSIM by different models on the test set of BSDS500 with different SNRs at different CS ratios of 30%, 10%, and 4%. It can be noticed that in most cases, the original model and the model with SDCS have similar performance, which demonstrates that SDCS will not weaken the anti-noise ability of the original model to a certain extent. The only exception is that AMP-Net outperforms AMP-Net-SDCS with a low SNR of 15dB, which means that the anti-noise performance of *model* may decline with a low SNR when it is combined with SDCS. Furthermore, combined with SDCS, a single model can be used to achieve sampling and reconstruction at multiple CS ratios, which further illustrates the advantage of SDCS.

Since *model*-RACS-1% has the most similar performance to *model*-SDCS in subsection 4.3, we compare *model*-RACS-1% with *model*-SDCS to further validate the anti-noise performance of SDCS. Fig. 7 shows the average PSNR and SSIM of CSNet<sup>+</sup>-SDCS, CSNet<sup>+</sup>-RACS-1%, AMP-Net-SDCS, AMP-Net-RACS-1% with different SNRs at CS ratios from 1% to 50%. In Fig. 4, when there is no noise, the maximum difference of the PSNR and the SSIM of *model*-SDCS and *model*-RACS-1% are 1dB and 0.04, respectively. It can be noticed from Fig. 7 that as the SNR decreases, the performance of each model decreases, and the performance difference between *model*-SDCS and *model*-RACS-1% also increases. In particular, the performance of CSNet<sup>+</sup>-SDCS with an SNR of 15dB is even better than *model*-RACS-1% with an SNR of 30dB, and for CSNet<sup>+</sup>-RACS-1%, the PSNR is even lower than 10dB and the SSIM is lower than 0.1, which may be due to that the traditional deep model combined with RACS cannot be well adapted to the condition of low SNR. Therefore, it can be concluded that SDCS has better anti-noise performance than RACS and is more suitable for imaging under actual conditions.

## 5 Conclusion

In this paper, for the visual image CS problem, we propose a general framework named SDCS to achieve SSR of deep-learning-based models. Besides of the initialization matrix and two sampling matrix masks, SDCS does not change the structure of the model. The proposed scalable training can generate an appropriate combination of the sampling matrix and the reconstruction model for efficient SSR. Experimental results show that SDCS outperforms other SSR methods. Specifically, models with SDCS can inherit the characteristics of the original models, e.g. the deblocking ability. In addition, it is shown that SDCS can work well with additive noises.

However, SDCS has one shortcoming:  $R_i$  being sampled uniformly during training makes the different training times of rows of the sampling matrix, which may affect the performance of SDCS. In the future, we will try to find a better way to generate  $R_i$  and try some bigger datasets like ImageNet (He et al., 2016) to improve the power of SDCS. Further more, we will extend SDCS to high-dimensional CS problems which demand SSR. For example, snapshot compressive imaging (SCI) (Liu et al., 2018; Ma et al., 2019) is promising to use a single model to reconstruct hyperspectral images in different frequency bands, and some applications like transient imaging (Sun et al., 2018) and magnetic resonance imaging (MRI) (Liu et al., 2017; 2020) can obtain images at different ratios using one model with a binary sampling matrix. As different CS applications have different sampling and reconstruction strategies, which makes the current SDCS has to be updated to adapt to them.

## References

- Pablo Arbelaez, Michael Maire, Charless Fowlkes, and Jitendra Malik. Contour detection and hierarchical image segmentation. *IEEE Transactions on Pattern Analysis and Machine Intelligence*, 33(5):898–916, 2010.
- Amir Beck and Marc Teboulle. A fast iterative shrinkage-thresholding algorithm for linear inverse problems. *SIAM Journal on Imaging Sciences*, 2(1):183–202, 2009.
- Ashish Bora, Ajil Jalal, Eric Price, and Alexandros G. Dimakis. Compressed sensing using generative models. In Doina Precup and Yee Whye Teh (eds.), *Proceedings of the 34th International Conference on Machine*

- Learning*, volume 70 of *Proceedings of Machine Learning Research*, pp. 537–546, International Convention Centre, Sydney, Australia, 06–11 Aug 2017. PMLR.
- Mark Borgerding, Philip Schniter, and Sundeep Rangan. AMP-inspired deep networks for sparse linear inverse problems. *IEEE Transactions on Signal Processing*, 65(16):4293–4308, 2017.
- Xiaohan Chen, Jialin Liu, Zhangyang Wang, and Wotao Yin. Theoretical linear convergence of unfolded ISTA and its practical weights and thresholds. In *Advances in Neural Information Processing Systems*, pp. 9061–9071, 2018.
- Khanh Quoc Dinh and Byeungwoo Jeon. Iterative weighted recovery for block-based compressive sensing of image/video at a low subrate. *IEEE Transactions on Circuits and Systems for Video Technology*, 27(11):2294–2308, 2017. doi: 10.1109/TCSVT.2016.2587398.
- Weisheng Dong, Guangming Shi, Xin Li, Yi Ma, and Feng Huang. Compressive sensing via nonlocal low-rank regularization. *IEEE Transactions on Image Processing*, 23(8):3618–3632, 2014.
- Weisheng Dong, Peiyao Wang, Wotao Yin, Guangming Shi, Fangfang Wu, and Xiaotong Lu. Denoising prior driven deep neural network for image restoration. *IEEE Transactions on Pattern Analysis and Machine Intelligence*, 41(10):2305–2318, 2018.
- David L Donoho, Arian Maleki, and Andrea Montanari. Message-passing algorithms for compressed sensing. *Proceedings of the National Academy of Sciences*, 106(45):18914–18919, 2009.
- Jiang Du, Xuemei Xie, Chenye Wang, Guangming Shi, Xun Xu, and Yuxiang Wang. Fully convolutional measurement network for compressive sensing image reconstruction. *Neurocomputing*, 328:105–112, 2019.
- Marco F Duarte, Mark A Davenport, Dharmpal Takhar, Jason N Laska, Ting Sun, Kevin F Kelly, and Richard G Baraniuk. Single-pixel imaging via compressive sampling. *IEEE Signal Processing Magazine*, 25(2):83–91, 2008.
- Michael Elad. *Sparse and redundant representations: from theory to applications in signal and image processing*. Springer Science & Business Media, 2010.
- Karol Gregor and Yann LeCun. Learning fast approximations of sparse coding. In *The 27th International Conference on International Conference on Machine Learning*, pp. 399–406. Omnipress, 2010.
- Jiajia Guo, Chao-Kai Wen, Shi Jin, and Geoffrey Ye Li. Convolutional neural network-based multiple-rate compressive sensing for massive mimo csi feedback: Design, simulation, and analysis. *IEEE Transactions on Wireless Communications*, 19(4):2827–2840, 2020.
- Kaiming He, Xiangyu Zhang, Shaoqing Ren, and Jian Sun. Deep residual learning for image recognition. In *The IEEE Conference on Computer Vision and Pattern Recognition*, pp. 770–778, 2016.
- Edward J. Hu, Yelong Shen, Phillip Wallis, Zeyuan Allen-Zhu, Yuanzhi Li, Shean Wang, and Weizhu Chen. Lora: Low-rank adaptation of large language models. *CoRR*, abs/2106.09685, 2021. URL <https://arxiv.org/abs/2106.09685>.
- Yixing Huang, Tobias Würfl, Katharina Breininger, Ling Liu, Günter Lauritsch, and Andreas Maier. Some investigations on robustness of deep learning in limited angle tomography. In *International Conference on Medical Image Computing and Computer-Assisted Intervention*, pp. 145–153. Springer, 2018.
- Diederik P Kingma and Jimmy Ba. ADAM : A method for stochastic optimization. *International Conference on Learning Representations*, 2015.
- OV Lepskii. On a problem of adaptive estimation in gaussian white noise. *Theory of Probability & Its Applications*, 35(3):454–466, 1991.
- Chengbo Li, Hong Jiang, Paul Wilford, Yin Zhang, and Mike Scheutzow. A new compressive video sensing framework for mobile broadcast. *IEEE Transactions on Broadcasting*, 59(1):197–205, 2013.

Yong Li, Wenrui Dai, Junni Zhou, Hongkai Xiong, and Yuan F. Zheng. Scalable structured compressive video sampling with hierarchical subspace learning. *IEEE Transactions on Circuits and Systems for Video Technology*, 30(10):3528–3543, 2020. doi: 10.1109/TCSVT.2019.2939370.

Yang Liu, Xin Yuan, Jinli Suo, David J Brady, and Qionghai Dai. Rank minimization for snapshot compressive imaging. *IEEE Transactions on Pattern Analysis and Machine Intelligence*, 41(12):2990–3006, 2018.

Yipeng Liu, Shan Wu, Xiaolin Huang, Bing Chen, and Ce Zhu. Hybrid CS-DMRI : Periodic time-variant subsampling and omnidirectional total variation based reconstruction. *IEEE Transactions on Medical Imaging*, 36(10):2148–2159, 2017.

Yipeng Liu, Zhen Long, Huyan Huang, and Ce Zhu. Low CP rank and Tucker rank tensor completion for estimating missing components in image data. *IEEE Transactions on Circuits and Systems for Video Technology*, 2019.

Yipeng Liu, Tengteng Liu, Jianli Liu, and Ce Zhu. Smooth robust tensor principal component analysis for compressed sensing of dynamic mri. *Pattern Recognition*, 102:107252, 2020.

Suhas Lohit, Kuldeep Kulkarni, Ronan Kerviche, Pavan Turaga, and Amit Ashok. Convolutional neural networks for noniterative reconstruction of compressively sensed images. *IEEE Transactions on Computational Imaging*, 4(3):326–340, 2018a.

Suhas Lohit, Rajhans Singh, Kuldeep Kulkarni, and Pavan Turaga. Rate-adaptive neural networks for spatial multiplexers. *arXiv preprint arXiv:1809.02850*, 2018b.

Jiawei Ma, Xiao-Yang Liu, Zheng Shou, and Xin Yuan. Deep tensor ADMM-Net for snapshot compressive imaging. In *Proceedings of the IEEE International Conference on Computer Vision*, pp. 10223–10232, 2019.

Chris Metzler, Ali Mousavi, and Richard Baraniuk. Learned d-amp: Principled neural network based compressive image recovery. In *Advances in Neural Information Processing Systems*, pp. 1772–1783, 2017.

Ali Mousavi, Ankit B Patel, and Richard G Baraniuk. A deep learning approach to structured signal recovery. In *The 53rd Annual Allerton Conference on Communication, Control, and Computing*, pp. 1336–1343. IEEE, 2015.

JH Rick Chang, Chun-Liang Li, Barnabas Poczos, BVK Vijaya Kumar, and Aswin C Sankaranarayanan. One network to solve them all—solving linear inverse problems using deep projection models. In *Proceedings of the IEEE International Conference on Computer Vision*, pp. 5888–5897, 2017.

Wuzhen Shi, Feng Jiang, Shaohui Liu, and Debin Zhao. Image compressed sensing using convolutional neural network. *IEEE Transactions on Image Processing*, 29:375–388, 2019a.

Wuzhen Shi, Feng Jiang, Shaohui Liu, and Debin Zhao. Scalable convolutional neural network for image compressed sensing. In *The IEEE Conference on Computer Vision and Pattern Recognition*, pp. 12290–12299, 2019b.

Wuzhen Shi, Shaohui Liu, Feng Jiang, and Debin Zhao. Video compressed sensing using a convolutional neural network. *IEEE Transactions on Circuits and Systems for Video Technology*, pp. 1–1, 2020. doi: 10.1109/TCSVT.2020.2978703.

Yueming Su and Qiusheng Lian. ipiano-net: Nonconvex optimization inspired multi-scale reconstruction network for compressed sensing. *Signal Processing: Image Communication*, 89:115989, 2020.

Jian Sun, Huibin Li, Zongben Xu, et al. Deep ADMM-Net for compressive sensing MRI . In *Advances in Neural Information Processing Systems*, pp. 10–18, 2016.

- Qilin Sun, Xiong Dun, Yifan Peng, and Wolfgang Heidrich. Depth and transient imaging with compressive spad array cameras. In *Proceedings of the IEEE Conference on Computer Vision and Pattern Recognition*, pp. 273–282, 2018.
- Yubao Sun, Jiwei Chen, Qingshan Liu, and Guangcan Liu. Learning image compressed sensing with sub-pixel convolutional generative adversarial network. *Pattern Recognition*, 98:107051, 2020.
- Zhengzhong Tu, Hossein Talebi, Han Zhang, Feng Yang, Peyman Milanfar, Alan Bovik, and Yinxiao Li. Maxvit: Multi-axis vision transformer. In *Computer Vision–ECCV 2022: 17th European Conference, Tel Aviv, Israel, October 23–27, 2022, Proceedings, Part XXIV*, pp. 459–479. Springer, 2022.
- Yibo Xu, Weidi Liu, and Kevin F Kelly. Compressed domain image classification using a dynamic-rate neural network. *IEEE Access*, 8:217711–217722, 2020.
- Chenggang Yan, Biao Gong, Yuxuan Wei, and Yue Gao. Deep multi-view enhancement hashing for image retrieval. *IEEE Transactions on Pattern Analysis and Machine Intelligence*, 2020a.
- Chenggang Yan, Zhisheng Li, Yongbing Zhang, Yutao Liu, Xiangyang Ji, and Yongdong Zhang. Depth image denoising using nuclear norm and learning graph model. *ACM Transactions on Multimedia Computing, Communications, and Applications (TOMM)*, 16(4):1–17, 2020b.
- Chenggang Yan, Biyao Shao, Hao Zhao, Ruixin Ning, Yongdong Zhang, and Feng Xu. 3d room layout estimation from a single rgb image. *IEEE Transactions on Multimedia*, 22(11):3014–3024, 2020c.
- Hantao Yao, Feng Dai, Shiliang Zhang, Yongdong Zhang, Qi Tian, and Changsheng Xu. Dr2-net: Deep residual reconstruction network for image compressive sensing. *Neurocomputing*, 359:483–493, 2019.
- Wenbin Yin, Xiaopeng Fan, Yunhui Shi, Ruiqin Xiong, and Debin Zhao. Compressive sensing based soft video broadcast using spatial and temporal sparsity. *Mobile Networks and Applications*, 21(6):1002–1012, 2016.
- Jian Zhang and Bernard Ghanem. ISTA-Net : Interpretable optimization-inspired deep network for image compressive sensing. In *The IEEE Conference on Computer Vision and Pattern Recognition*, pp. 1828–1837, 2018.
- Zhikang Zhang, Kai Xu, and Fengbo Ren. CRA: A generic compression ratio adapter for end-to-end data-driven image compressive sensing reconstruction frameworks. In *ICASSP 2020-2020 IEEE International Conference on Acoustics, Speech and Signal Processing (ICASSP)*, pp. 1439–1443. IEEE, 2020.
- Zhonghao Zhang, Yipeng Liu, Jianli Liu, Fei Wen, and Ce Zhu. Amp-net: Denoising-based deep unfolding for compressive image sensing. *IEEE Transactions on Image Processing*, 30:1487–1500, 2021. doi: 10.1109/TIP.2020.3044472.